Computers and Geotechnics 36 (2009) 1024–1038

Contents lists available at ScienceDirect

Computers and Geotechnics

journal homepage: www.elsevier.com/locate/compgeo

Simulation of the progressive failure of an embankment on soft soil

Jinchun Chai [a,*], John P. Carter [b]

[a] Department of Civil Engineering, Saga University, 1 Honjo, Saga 840-8502, Japan
[b] Faculty of Engineering and Built Environment, The University of Newcastle, Australia

ARTICLE INFO

Article history:
Received 3 June 2008
Received in revised form 5 January 2009
Accepted 23 March 2009
Available online 24 April 2009

Keywords:
Progressive failure
Finite element analysis
Constitutive model
Case history

ABSTRACT

A pragmatic strain-softening constitutive model, which is based on Modified Cam Clay, was applied to the simulation of the progressive failure of an embankment constructed on a deposit of sensitive (strain-softening) clay in Saga, Japan. A comparison of the predictions for this case indicates that if softening is ignored, only relatively small deflections and consolidation settlements are predicted, especially after construction. In contrast, for the case where softening is included in the analysis, progressive failure within the clay induces large shear deformations and finally failure of the embankment is predicted. This comparison suggests that softening-induced progressive failure should be considered in the design of embankments on such soils, and the residual strength of the deposit may have an important influence on the overall factor of safety of the construction. Detailed analyses of predicted excess pore water pressures, shear strains and shear stress levels in the ground indicate that considering the strain-softening process: (a) is associated with the buildup of excess pore water pressure; (b) promotes strain localization; and (c) results generally in a larger zone of soil involved in the failure.

1. Introduction

Many natural clay deposits exhibit some strain-softening behaviour, which can affect, for example, the stability of an embankment and the bearing capacity of a foundation constructed on this kind of ground. For a deposit with strain-softening characteristics, using its peak strength in design even with a factor of safety (FS) around 1.5 may still result in failure of the structure due to progressive softening of the foundation soil. An example of this situation is the case of the Carsington embankment in the UK [11]. On the other hand, if the residual strength of the clay is used in design, particularly for some very sensitive deposits, the design may be overly conservative. The mobilized strength in a clayey deposit depends, amongst other factors, on the construction speed and the scale of the structure, and so in order to arrive at a safe and economic design it is desirable to investigate the effect of the strain-softening on the response of the foundation soils and the behaviour of the structure. This is most conveniently achieved using a numerical analysis that takes strain-softening into account.

Most existing elasto-plastic soil models for clayey soils have limited capacity to model strain-softening behaviour. For example, when considering undrained conditions, the widely used Modified Cam Clay (MCC) model [12] can only simulate softening for a soil element in a heavily over-consolidated state with a relatively high value of the ratio κ/λ, where λ and κ are, respectively, the slopes of the virgin loading and the unloading–reloading lines in $e - \ln p'$ space (e is void ratio and p' is mean effective stress). However, some normally consolidated clay soils also exhibit strain-softening. In order to include the effects of softening more generally Chai et al. [7] proposed a pragmatic approach, based on the MCC model, to simulate the strain-softening behaviour of clay soils under undrained or partially drained conditions.

In this paper, the method proposed by Chai et al. [7] is applied to the simulation of an embankment on strain-softening soil at Saga in Japan. In this field case the embankment ultimately failed, as reported by Takayama et al. [14]. By comparing the predictions of finite element analyses in which strain-softening was included with the predictions for the case where it was ignored, the effects of the strain-softening on the response of the foundation soil and the embankment behaviour have been identified.

2. Case history of embankment failure

2.1. Site conditions

Around the Ariake Sea in Japan there is a thick soil deposit known as Ariake clay. This area is famous in Japan for growing rice. However, largely due to mining-induced land subsidence, the ground surface had been lowered in some places. In order to raise the surface elevation and to improve the irrigation system, canals and creeks, some greater than 2 m deep, were constructed during the 1970s by excavation, often in conjunction with the construction of an adjacent road embankment. Due to the low strength of

* Corresponding author. Tel.: +81 952 28 8580; fax: +81 952 28 8190.
E-mail address: chai@cc.saga-u.ac.jp (J. Chai).

0266-352X/$ - see front matter © 2009 Elsevier Ltd. All rights reserved.
doi:10.1016/j.compgeo.2009.03.010

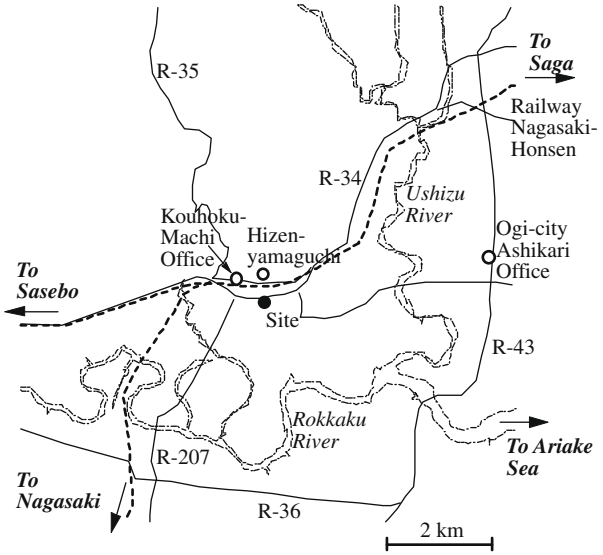

Fig. 1. Location of the site.

Ariake clay there were several reported cases of failure of these embankments [14]. One of the failure cases was analyzed in this study to investigate the mechanism of progressive failure involving strain-softening of the foundation soil.

The site considered in this study is located in Kouhoku-Machi, Saga, Japan (Fig. 1). At this site, the very soft Ariake clay deposit is about 15 m thick and the soil profile is as given in Fig. 2 (data from Takayama et al. [14]). It can be seen that the natural water content was generally 100–150% and larger than the corresponding liquid limit. In the upper layer (about 6 m thick), the undrained shear strength was about 10 kPa.

2.2. Brief description of embankment failure

The geometry of the embankment studied here is shown in Fig. 3 (modified from Takayama et al. [14]). Fig. 3b shows the dimensions of the embankment before failure. An existing canal about 1.0 m deep was deepened by excavation to about 1.6 m and a small road embankment was constructed just beside the canal. At the toe of the embankment approximately 4 m long wooden-piles were installed to increase the stability of the embankment. The diameters of the wooden-piles were 0.17–0.20 m at the head and about 0.15 m at the base, with an average diameter of approximately 0.17 m. The center-to-center spacing between adjacent piles was about 1.0 m. Within the top 1.0 m of these piles, logs with a diameter of about 0.1 m were laid horizontally behind the piles to form a wooden wall. A 0.3 m by 0.3 m reinforced concrete-beam was constructed on the head of these piles (Personal communication with Dr. R. Nakamura, the second author of the paper by Takayama et al. [14]). At the site, the elevation of the farm land was raised by first stripping the top soil and filling with fine sandy soil. The top soil was replaced and then the canal was deepened and an embankment was constructed. Details of the construction history are listed in Table 1.

3. Material properties

3.1. Foundation soil

To investigate the mechanism of failure, boreholes were drilled and undisturbed soil samples were obtained from the slide body (Fig. 3a) and from an adjacent area that had not experienced failure. A series of laboratory unconfined compression tests and limited triaxial unconsolidated and undrained (UU) compression tests as well as consolidation tests were conducted on the undisturbed samples. Fig. 4a–c compare the stress–strain relationships observed in the unconfined compression tests for soil samples recovered at depths of 2.8, 4.7 and 6.0 m, respectively, from the no-failure area (designated as "Before failure") and beneath the failed embankment (designated as "After failure"). It can be seen that the compressive strength measured in the unconfined compression tests (q_u) reduced significantly after failure at approximately 4.7 m depth. All unconfined compression test results, expressed in terms of the measured undrained shear strength ($S_u = q_u/2$) and the axial strain (ε_f) corresponding to the peak strength, are summarized in Fig. 5. From these results it can be inferred that the failure surface was located at a depth of about 4.7 m at the location of the borehole (see Fig. 3a). Based on the observed locations of cracks and the test results shown in Fig. 5, the locations of the slip surfaces estimated both by Takayama et al. [14] and the writers are as indicated in Fig. 3a.

The results in Fig. 4b indicate that the failure process would have involved strain-softening. The value of q_u after failure was about 50% of the peak value. To investigate further the strain-softening process, a UU triaxial compression test with a confining pressure of 49 kPa was conducted for the soil samples recovered at a depth of 4.7 m beneath the no-failure area, and the results are gi-

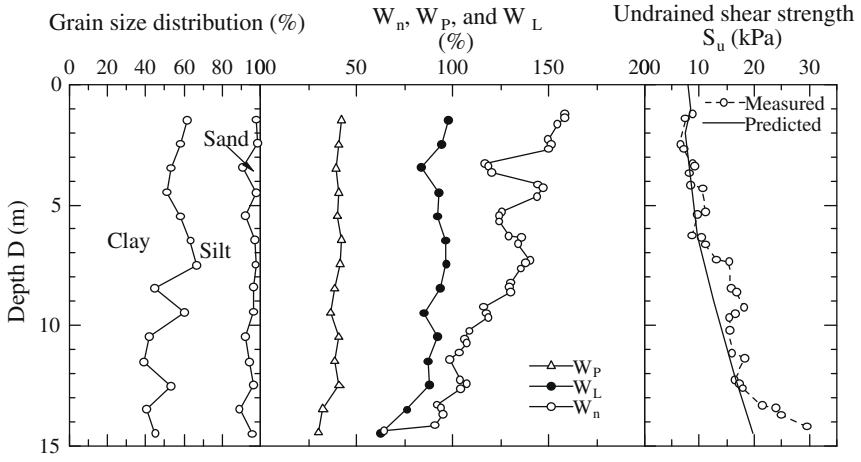

Fig. 2. Soil profile at the site (data from Takayama et al. [14]).

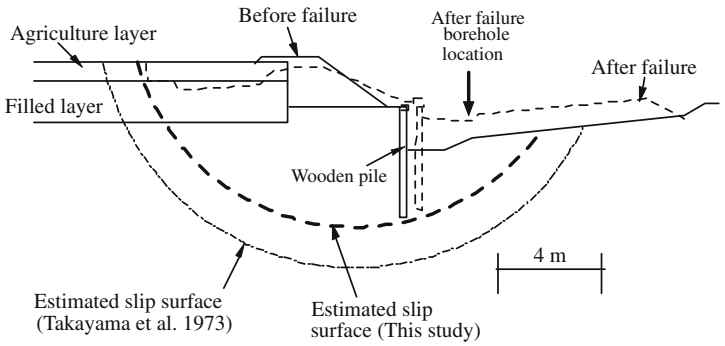

(a) Embankment shape before and after failure

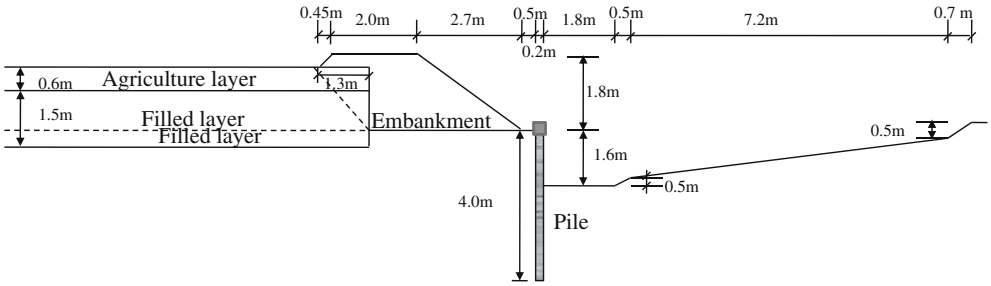

(b) Dimension of the embankment system before failure

Fig. 3. Geometry of the embankment before and after failure.

Table 1
Actual construction history (after Takayama et al. [14]) and simulated construction procedures.

Actual			Simulated		
Date	Period (days)	Activities	Stage	Period (days)	Methods
–	–	Excavating the old canal (1 m deep)	1	365	No nodal coordinate update and at the end erase all the displacement
7 – 10/12/1970	4	Removing surface farming soil layer			Excavating and replacing the farming soil layers were not simulated. Assume 10 days for back filling the equivalent excavated farming soil layers
11 – 29/12/1970	19 (overlap)	Removing subsurface farming soil layer			
17/12/1970 – 12/01/1971	26 (overlap)	Filling the fine soil			
7/01/1971 – 7/02/1971	70 (overlap)	Back filling the subsurface farming soil	2	30	Construction of 1.0 m thick fill (update nodal coordinates)
19/01/1971 – 23/03/1971		Back filling the surface farming soil	(5)		Due to the overlapping of the activities, the remaining 0.5 m filling is simulated after wooden-pile installation and canal deepening
7/02/1971	–	Installing the wooden-pile and concrete-beam system	3	1	Change the properties of the corresponding solid elements from an elasto-plastic to an elastic material
3/02/1971	–	Excavating the canal (from 1.0 m deep to 1.6 m deep)	4	5	The canal was excavated from 1.0 m to 1.6 m below the ground surface by removing the corresponding elements
7/02/1971	–	Back filling the retaining side around the piles	5	50	In the actual construction, the farming soil layer was returned, but in simulation, additional 0.5 m fill material was added. The farming road was 0.3 m higher than the farming field
8/02/1971	–	Constructing the road embankment			
24/03/1971 – 11/04/1971	19	Consolidation and progressive failure	6	19	Consolidation and strain-softening
11/04/1971	–	Slope failure			

ven in Fig. 6. It can be seen that the peak strength was mobilized at about 3% axial strain and the residual strength was reached at about 7% axial strain, with a magnitude equivalent to about 70% of the peak strength. It is considered that the result of the UU test is more reliable than that of the unconfined compression tests, and in the following finite element analyses the strain-softening parameters for the deposit were estimated using the results shown in Fig. 6.

Results of a consolidation test on a sample from the no-failure area at a depth of 4.7 m are shown in Fig. 7, from which a compression index (C_c) of about 1.4 can be estimated. The measured values of coefficient of consolidation (C_v) were 0.03–0.04 m^2/day in the

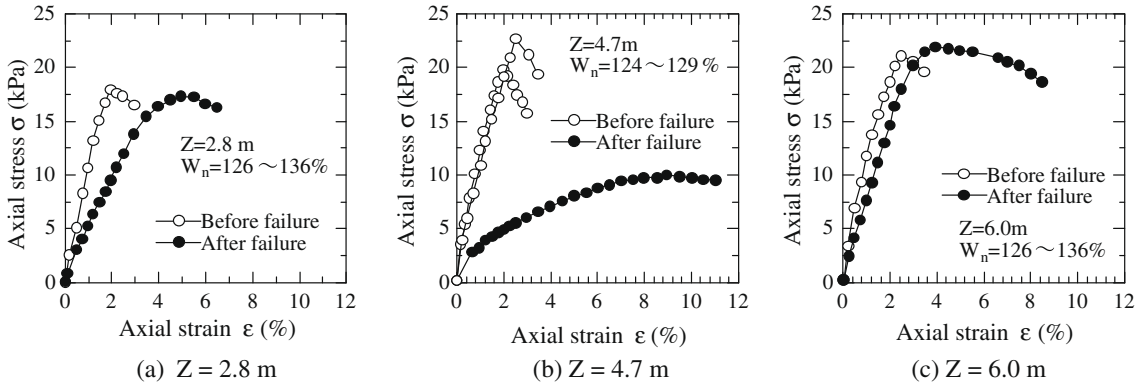

Fig. 4. Strain–stress curves of unconfined compression tests (data from Takayama et al. [14]).

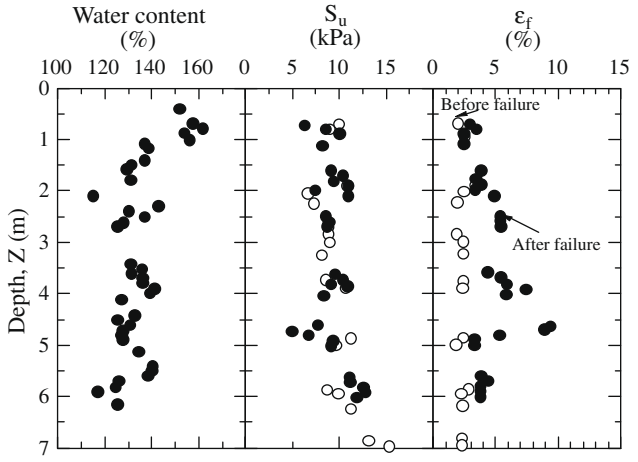

Fig. 5. Variation of water content, undrained shear strength and axial strain at peak strength with depth (data from Takayama et al. [14]).

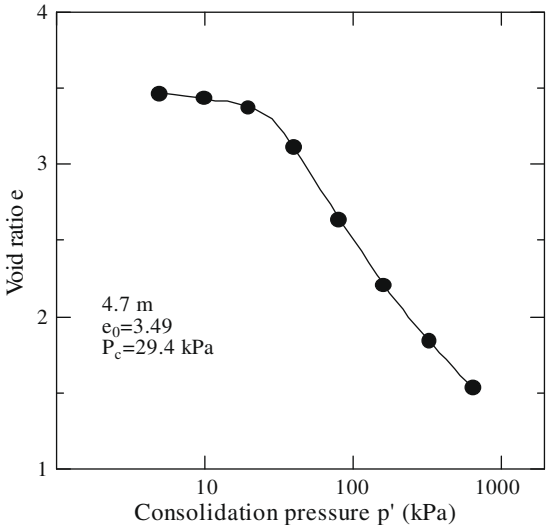

Fig. 7. Consolidation curve for the sample at 4.7 m depth.

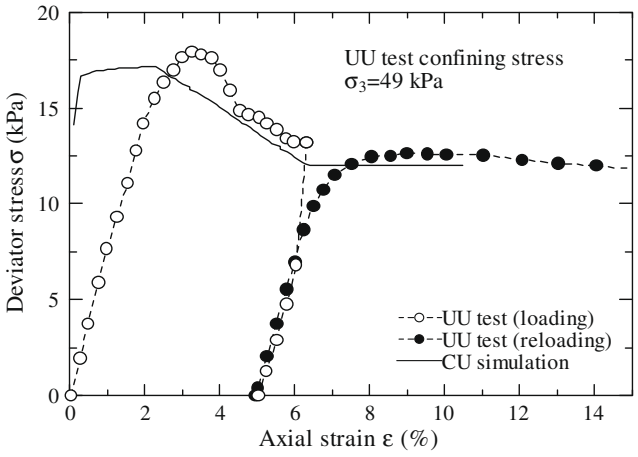

Fig. 6. UU triaxial test and CU simulation results (test data from Takayama et al. [14]).

Table 2
Physical properties of fill material (data from Takayama et al. [14]).

Property	At the end of construction	After failure
Water content, W_n (%)	31–32	31–35
Total unit weight γ_t (kN/m^3)	17.2–17.3	1.72–17.6
Dry unit weight γ_d (kN/m^3)	13.1	13.1
Degree of saturation S_r (%)	85	85–91 (88)
Cohesion C_u (kPa)	9.0	7.3
Friction angle ϕ_u (°)	6.3	4.8

over-consolidated range and 0.005–0.007 m^2/day in the normally consolidated range. Considering the over-consolidation range and using $e = 3.5$ and $\sigma_{v0} = 19.8$ kPa and $C_v = 0.04$ m^2/day, a value of hydraulic conductivity of 3.16×10^{-9} m/s can be deduced.

3.2. Fill material

The physical properties of the fill material are listed in Table 2. Takayama et al. [14] conducted UU triaxial compression tests on the compacted fill material with a dry unit weight of 13.1 kN/m^3 and different degrees of saturation. The results are summarized in Fig. 8. The values of apparent cohesion C_u and apparent friction angle ϕ_u of the unsaturated fill have been interpreted from Fig. 8 and are listed in Table 2.

4. Bearing capacity calculation and slip circle analysis

Before conducting finite element (FEM) simulations of the embankment loading and failure, it was worthwhile to estimate

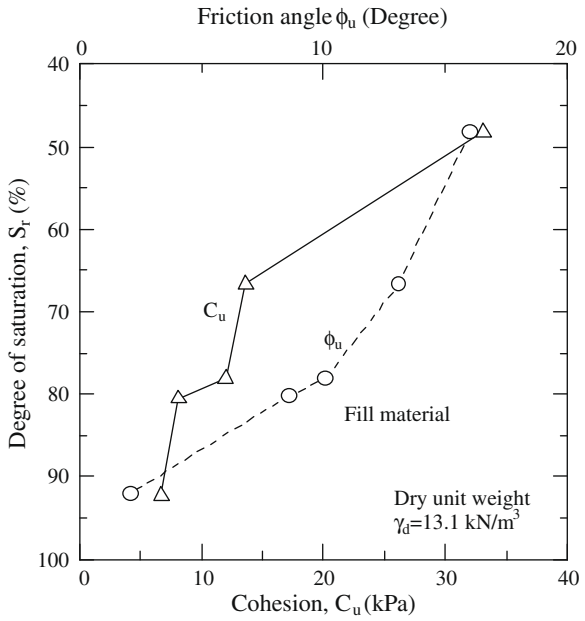

Fig. 8. Variation of cohesion and friction angle with degree of saturation of the fill material (data from Takayama et al. [14]).

the ultimate bearing capacity (q_{ult}) of the foundation soil under undrained conditions. As shown in Fig. 2, the undrained shear strength (S_u) of the deposit increases with depth. Davis and Booker [8] published solutions that may be used to calculate values of q_{ult} for surface footings on soils with S_u increasing linearly with depth:

$$S_u = S_{u0} + \rho \cdot z \quad (1)$$

where S_{u0} is the value of undrained shear strength at the ground surface, ρ is the rate of strength increase with depth, and z is depth. From the test data shown in Fig. 2, S_{u0} = 6.4 kPa and ρ = 0.5 kPa/m can be estimated. However, since there was an excavation just beside the toe of the embankment with a depth from about 0.5–1.6 m and an average depth of about 1.0 m, it could be argued that it would be more appropriate to consider the 1.0 m thick surface layer effectively as an additional surcharge. In this case at 1.0 m depth a value of S_{u0} = 6.9 kPa would be more appropriate.

The width of the failure zone from the wooden-pile to the failure surface in the fill material (left side in Fig. 3a) is about 12 m. Considering this as the half width of an equivalent "footing", an ultimate bearing capacity of q_{ult} = 52.5 kPa can be calculated using the solutions of Davis and Booker. If strain-softening is considered and a reduced value of S_{u0} = 4.8 kPa (70% of the peak value of 6.9 kPa) is adopted, then q_{ult} = 40.4 kPa is calculated. The surcharge loading, including the weight of the embankment fill, is estimated

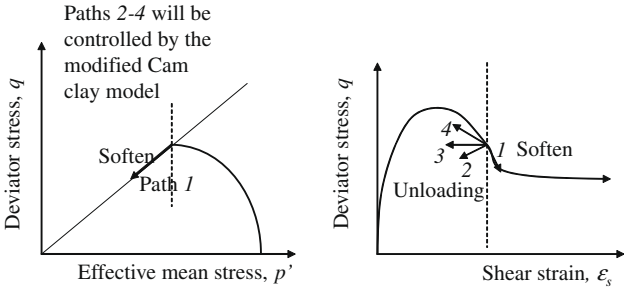

Fig. 9. Possible stress paths after stress state passes the peak.

as being between 41 and 46 kPa, which exceeds the value of q_{ult} computed for the softening case.

Simple calculations of this type indicate that if the foundation soil does not exhibit softening behaviour, then the embankment system acting as a footing load would not be predicted to fail. However, if softening is taken into account and a mobilized strength equivalent to 70% of the peak value is assumed, then the factor safety of the embankment when regarded as an equivalent footing is calculated as less than unity and the embankment is predicted to fail.

Using the values of S_u shown in Fig. 2 for the subsoil layers and C_u = 9.0 kPa and φ_u = 6.3 (Table 2) for the fill material, as well as the total unit weights given in Table 3, slip circle analyses using Bishop's method were also conducted. The resulting minimum factor of safety (FS) is 1.22. However, if values of C_u = 7.3 kPa and φ_u = 4.8° are adopted (as in Table 2 for conditions after failure), and 70% of the undrained shear strength values indicated in Fig. 2 for the subsoil layers are adopted, a value of FS = 0.88 was obtained. In this case the slip circle corresponding to the minimum FS just passes the tips of the wooden-piles (about 4 m deep), which is shallower than the estimated field slip circle suggested by Takayama et al. [14]. Although the values of FS from the slip circle analyses are not exactly the same as those obtained by the bearing capacity analysis, both analyses indicate the same trend, viz., if no strain-softening had been involved it is unlikely that the slope would have failed.

5. Simulating embankment behaviour

The embankment was analyzed by the FEM to investigate the effect of strain-softening on progressive failure. In the analyses, the Ariake clay was represented by the Modified Cam Clay (MCC) model [12] for the cases that include and ignore softening, and the embankment fill material was simulated by a linear elastic model. Since there is no information indicating strain-softening behaviour in the fill material, only softening of the soft foundation

Table 3
Soil parameters for finite element analysis.

Depth (m)	Soils	E (kPa)	ν	SR, C_u (kPa)	$\Delta\varepsilon_{sL}$, ϕ_u (°)	κ	λ	M	e_0	γ_t (kN/m^3)	k_h (10^{-8} m/s)	k_v (10^{-8} m/s)
0.0–1.0	Surface layer	–	0.3	0.7	0.04	0.04	0.43	1.2	2.9	14.0	1.50	1.00
1.0-2.0	Silty clay	–	0.3	0.7	0.04	0.07	0.69	1.2	4.1	13.0	4.54	3.03
2.0–6.3		–	0.3	0.7	0.04	0.06	0.61	1.2	3.5	13.4	1.50	1.00
6.3–9.0		–	0.3	0.7	0.04	0.06	0.61	1.2	3.3	13.5	1.20	0.80
9.0–12.0		–	0.3	0.7	0.04	0.05	0.52		2.9	13.9	0.62	0.41
12.0–14.5		–	0.3	0.7	0.04	0.04	0.43	1.2	2.5	14.4	0.32	0.21
14.5∼	Gravelly sand	20,000	0.25	10	35	–	–	–	–	18.0	290	290
Fill		2000	0.30	10	6	–	–	–	–	18.0	15.0	10.0

Note: E, Young's modulus; ν, Poisson's ratio; λ, slope of consolidation line in $e - \ln p'$ plot; κ, slope of unloading–reloading line in $e - \ln p'$ plot; M, slope of critical state line in p'–q plot (q is deviator stress); e_0, initial void ratio; γ_t, unit weight; k_v and k_h are hydraulic conductivities in vertical and horizontal directions respectively; SR and $\Delta\varepsilon_{sL}$ are strain-softening parameters; and C_u and ϕ_u are undrained cohesion and friction angle.

soil was considered using the method proposed by Chai et al. [7]. This method is briefly summarized below.

5.1. Strain-softening model

The soil model proposed by Chai et al. [7] is a simple extension of MCC. In this model it is assumed that during softening the strain increments can still be calculated according to the MCC model, i.e., there is no volumetric strain increment ($\Delta\varepsilon_v = 0$) and the shear strain increment ($\Delta\varepsilon_s$) is indefinite. In a boundary value problem the shear strain will be limited by (external) kinematic conditions. However, the effective stress path is forced to follow the projection of the critical state line (CSL) in a p'–q plot (i.e., $q = M\,p'$, where q is deviator stress and M is the slope of the CSL in the p'–q plot). This enforcement of the softening stress path is based on experimental evidence which indicates that during undrained triaxial tests the effective stress path during the softening phase is often close to the projection of the CSL in a p'–q plot [1,15].

The conditions for enforcing strain-softening are: (a) the stress state is on a current yield surface and on the CSL and (b) the shear strain is increasing and larger than the past maximum shear strain a soil element has experienced. As shown in Fig. 9, if the incremental shear strain $\Delta\varepsilon_s > 0$ (path 1 in Fig. 9), then strain-softening will occur. If $\Delta\varepsilon_s \leqslant 0$ (paths 2, 3 and 4 in Fig. 9), there will be no enforced strain-softening and the stress–strain relationship of a soil element will be fully controlled by the MCC model.

In effect, the soil retains a memory of the maximum shear strain it has experienced. Unloading from a softening state is an elastic process, but during reloading, when the shear strain again exceeds the maximum shear strain previously experienced and the stress state is on the current yield surface and on the CSL, softening will commence once again.

During softening it is assumed that for an incremental shear strain, $\Delta\varepsilon_{sL}$, the deviator stress reduces towards a residual value by an amount Δq, as shown in Fig. 10. When the stress state is on a current yield surface and on the CSL, most of the incremental shear strain will be plastic. However, for mathematical convenience the increment of total shear strain, $\Delta\varepsilon_{sL}$, is used to define the rate of softening.

In Fig. 10, ε_{scs} and q_{cs} are the shear strain and the deviator stress when the stress state first reaches the CSL and is also on a current yield surface. They are determined by the MCC model and not predefined. Since for general loading cases q_{cs} is not known, the value of Δq can not be properly specified *a priori*. Therefore, it is more convenient to use a ratio (SR) between the residual deviator stress q_{re} and q_{cs} as follows:

$$SR = \frac{q_{re}}{q_{cs}} \tag{2}$$

so that $\Delta q = (1 - SR)\cdot q_{cs}$. $\Delta\varepsilon_{sL}$ and SR will be used as two additional model parameters defining the strain-softening.

Following Carter and Liu [3], it is assumed that during strain-softening, the yield surface contracts and the effective stress path is only allowed to move along the CSL. If the stress states at the beginning and the end of a load increment, are denoted as (q_b, p'_b) and (q_e, p'_e), respectively, then $q_e = q_b + \Delta q$ and $p'_e = p'_b + \Delta p'$ ($\Delta p' = \Delta q/M$). However, for two dimensional (2D) problems the state of stress is necessarily described by four (4) quantities, while for three dimensional (3D) problems six (6) are required. Knowing only q_e and p'_e, i.e., two stress quantities only, the general stress state at the end of a load increment can not be determined.

In order to overcome this difficulty it is assumed that during softening all stresses reduce by the same proportion with respect to their values at the beginning of a load increment. For a 2D problem, this assumption can be expressed as follows:

$$\frac{\sigma'_{xe}}{\sigma'_{xb}} = \frac{\sigma'_{ye}}{\sigma'_{yb}} = \frac{\sigma'_{ze}}{\sigma'_{zb}} = \frac{\tau_{xye}}{\tau_{xyb}} = \frac{q_e}{q_b} \tag{3}$$

where $\sigma'_x, \sigma'_y, \sigma'_z$ are effective normal stresses in the x, y and z directions, respectively, and τ_{xy} is the shear stress in the x–y plane. Eq. (3) represents four linear equations from which the stress state at the end of a load increment can be obtained in terms of general stress variables. Obviously, for a drained triaxial test, linear reduction of stresses is not applicable when the effective confining stress does not change. For undrained or partially drained triaxial tests, linear reduction of stresses is possible. Therefore, the proposed method is limited to undrained or partially drained loading conditions.

With the method described above, the stress state at the end of a load increment is enforced so that overall force equilibrium is not guaranteed. To maintain equilibrium of a computed stress field, iteration of this process may be required. Equilibrium is checked at each load step by inspecting the nodal forces. The arbitrary criterion adopted is that any unbalanced nodal force is less than 1% of the maximum nodal force or the number of iterations reaches 20. Generally, small load increments are adopted, typically corresponding to placement of a layer of fill 0.05 m thick.

The proposed method has been incorporated into the CRISP–AIT program [4], which is based on the original CRISP program [2], and it has been applied successfully in the past to the simulation of the strain-softening behaviour of a natural Ariake clay and a lime stabilized Arikae clay [7]. To ensure that the true stress–strain law is followed closely in the numerical model, the Newton–Raphson method with an explicit sub-stepping technique that includes error control [13] has been incorporated into the program, in order to integrate the stresses in the elasto-plastic range. Using a Sun work station with a 1.35 GHz UltraSparc processor the simulation of the problem described here took about 1 h of processor time.

5.2. Model parameters

The adopted model parameters are listed in Table 3 and the assumed initial stresses in Table 4. The value of 2000 kPa for Young's modulus of the fill material was estimated as about 200 times its apparent cohesion, C_u. In Table 4, an initial value of 5 kPa horizon-

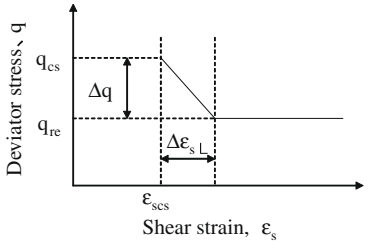

Fig. 10. An empirical shear strain versus deviator stress relationship.

Table 4
Initial stress in the subsoil.

Depth (m)	σ'_{h0} (kPa)	σ'_{v0} (kPa)	Size of yield locus p'_y (kPa)
0	5	0	27.8
1	7.0	14	27.8
2.0	8.6	17.2	23.5
6.3	16.3	32.68	30.3
9.0	21.3	42.67	39.6
12.0	27.5	54.97	51.0
14.5	33.2	66.47	61.6
20.0	55.8	111.57	103.4

tal effective stress is assigned at the ground surface in order to avoid zero or very close to zero effective mean stress for integration points located very closed to the ground surface, and therefore to avoid unrealistically low values being calculated by the model for the stiffness and strength at these shallow locations.

The division of the soil into different layers was made based on the natural water contents, as presented in Fig. 2. For the MCC parameters, firstly, the initial void ratio (e_0) was evaluated from the natural water content (Fig. 2) assuming 100% degree of saturation and a unit weight of the soil particles of 26.0 kN/m^3. For all layers, an effective stress friction angle $\varphi' = 30°$ was assumed, resulting in a value of M of 1.2. As mentioned previously, only the consolidation test results at 4.7 m depth were reported by Takayama et al. [14]. In the Kouhoku area of Saga in Japan, experience has shown that generally soil layers with a larger e_0 value have a larger λ value, and for clay layers near the gravelly sand layer, the λ value is about 0.35–0.43 [6]. Based on this information and the measured λ value at 4.7 m depth and data from a nearby site [6], the λ values for all layers except the surface layer were estimated. The surface layer is stiffer and unfortunately no test data is available. Therefore a λ value of 0.43 had to be assumed. In all cases the value of κ was assumed as 0.1 λ.

A value of hydraulic conductivity of $k_v = 1.0 \times 10^{-8}$ m/s was assumed for the soil at 4.7 m depth with a corresponding void ratio of $e = 3.5$. This value is about three times the value calculated from the consolidation test results, but it is well known that laboratory test will generally underestimate the field hydraulic conductivity since they cannot usually consider the effects of natural stratification on a field clay deposit. In this region, experience has shown that generally the field values are about 2–4 times the corresponding laboratory values [6]. At other depths the corresponding k_v values were calculated according to their void ratios by using Taylor's [16] equation with reference to the value at 4.7 m depth, i.e.,

$$k = k_0 \cdot 10^{-(e_0 - e)/C_k} \tag{4}$$

where k_0 is the initial hydraulic conductivity, e_0 is the initial void ratio, k is the current hydraulic conductivity, e is the current void ratio, and C_k is a constant. It has been found that using $C_k = 0.4e_0$, Eq. (4) worked very well for soft Ariake clay [5,6] and so this value was used in the present study. For the surface soil layer a value of $k_v = 1.0 \times 10^{-8}$ m/s was assumed. It was further assumed that the hydraulic conductivity of the embankment fill is 10 times that of the surface soil layer. For all clay layers the value of the horizontal hydraulic conductivity, k_h, was assumed to be 1.5 times the corresponding vertical value [10]. To investigate the effect of the adopted values of hydraulic conductivity (k), and therefore the resulting coefficient of consolidation, on the simulated performance of the embankment, a limited parametric study was conducted assuming k values between 0.5 and 1.5 times the values listed in Table 3. The outcomes of this limited study are discussed below.

In the field the wooden-pile and concrete-beam system acted as a retaining wall. In the plane strain analysis the row of wooden-piles was modelled as a wall by solid elements and an equivalent Young's modulus of the wall (E_{wall}) was calculated based on equal bending resistance, so that:

$$E_{wall} = \frac{3 \cdot \pi \cdot D^4}{16 \cdot B^3} N \cdot E_{pile} \tag{5}$$

where E_{pile} is Young's modulus of the wooden-pile, D is the diameter of the pile, N is the number of the piles per unit width, and B is the thickness of the wall. For the case considered $N = 1$ (i.e., the spacing between two adjacent piles was 1.0 m), $D = 0.17$ m, and $B = 0.2$ m. By adopting $E_{pile} = 8 \times 10^5$ kPa [9], $E_{wall} \cong 49,000$ kPa can be obtained. Considering the fact that the failure surface occurred below the wooden-pile and there was no large relative displacement observed in the field, no joint elements were employed between the wall and the surrounding soil.

In the strain-softening model, there are two additional softening parameters needed, i.e., $\Delta\varepsilon_{sL}$ and SR [7]. To calibrate these two parameters, an elemental simulation considering a soil sample at 4.7 m depth was conducted. To calculate the initial effective stresses in the soil element it was assumed that the groundwater level was 1.0 m below the ground surface, and a value of at rest earth pressure coefficient, k_o, of 0.5 was adopted.

As shown in Fig. 7, the maximum consolidation pressure for the undisturbed sample at 4.7 m depth is about 29.4 kPa, and an apparent over-consolidation ratio of about 1.2 can be estimated. With these parameters, an undrained shear strength (S_u) of 8.8 kPa is predicted by the MCC model, which is close to the measured value given in Fig. 2. Most soft clayey deposits have a crust layer at the ground surface. For the case considered here, part of the crust was excavated and back-filled by fine sandy soil with an apparent cohesion of about 9 kPa (Table 2). The simulated undrained shear strength of about 9 kPa (Fig. 2) therefore seems reasonable. The parameters for the elemental simulation are listed in Table 5. The simulated axial strain versus deviator stress curve is included in Fig. 6 for comparison. In the FEM analysis, there are difficulties in simulating a UU triaxial compression condition using the MCC model (it is unclear what initial effective stress state should be assigned to the sample). Instead, the simulation was made assuming consolidated undrained (CU) triaxial compression. The simulated peak strength and the amount of softening are close to the UU triaxial test results, but the initial stiffness is different from that of the tested UU condition. From this comparison, it is considered that the adopted strain-softening parameters, $SR = 0.7$ and $\Delta\varepsilon_{sL} = 0.04$, are reasonable and they were therefore used in simulating the behaviour of the embankment.

In the field construction, there were overlaps of some of the activities and for some activities only the start times were recorded (Table 1). In the FEM simulation, the construction process was simplified as in Table 1, and the process of excavating and restoring the top soil layer was not considered. As indicated in Table 1, the fieldwork involved in removing the top soil layer used for farming started on December 7, 1970 and back filling of the fine soil started on December 17, 1970 and ended on March 23, 1971, with a total filling duration of about 96 days. Assuming the time for placement of the fine soil layer, equivalent to the top soil layer, was 10 days, then the simulated field construction duration is estimated as 86 days (Table 1). About 19 days after embankment construction, on April 11, 1971, the embankment failed.

The FEM mesh and boundary conditions adopted in the simulation are shown in Fig. 11. Eight-noded quadrilateral and six-noded triangular elements were used; a few six-noded triangular elements are located around the excavation zone (Fig. 11) and some six-noded triangular elements have also been excavated. In a zone beneath and around the road embankment and the canal, the size

Table 5
Model parameters for elemental simulation.

Parameter	λ	κ	e_0	M	ν	$\Delta\varepsilon_{sL}$	SR	σ'_{h0} (kPa)	σ'_{v0} (kPa)	p'_{y0} (kPa)
Value	0.61	0.06	3.45	1.2	0.3	0.04	0.7	12.5	24.9	27.8

Note: σ'_{h0} and σ'_{v0} are initial horizontal and vertical effective stresses, respectively.

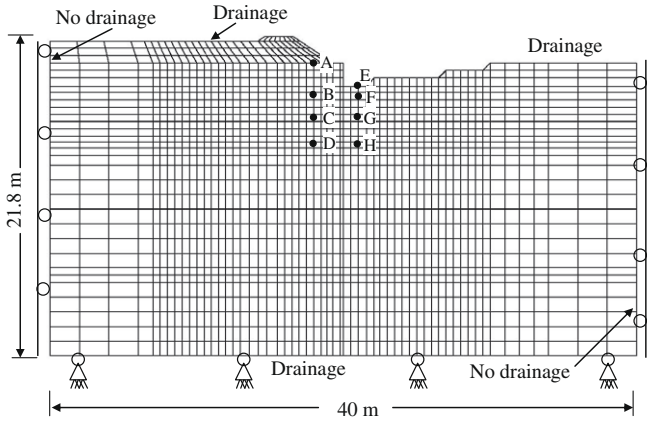

Fig. 11. FEM mesh and boundary conditions.

of the elements is basically 0.5 m in both the vertical and the horizontal directions. Theoretically, this mesh can simulate a shear band approximately 0.25 m wide. Two cases of simulation with and without considering the enforced strain-softening were conducted using this mesh and the results are compared in the following section. These two cases will be referred to as the softening and no-softening cases, respectively. It is important to note that the simulated initial undrained shear strength is potentially the same in each analysis, so that if the same pre-peak stress paths were followed, the mobilized peak strengths would be identical. However, since strain-softening is likely to alter the effective stress paths in a boundary value problem, the mobilized peak strengths at identical locations may not be exactly the same in the two types of analysis.

It is generally considered that for a strain-softening analysis the results may be mesh size dependent. Initially, analyses were also conducted with a coarser mesh, adopting a 1.0 m grid spacing in both the vertical and the horizontal directions. Comparison of the results of the two sets of analyses conducted with the coarser and finer meshes provided a simple check on the sensitivity of the predictions to the mesh size. It was found that for the no-softening case, there was no significant difference in the predicted results. However, there were some differences observed in the case of a softening soil. With the coarser mesh at the bottom of the wooden-piles (at 4.0 m depth), the predicted shear strains were not large enough to cause softening, but with the finer mesh they were (a comparison will be given later in the paper).

Unfortunately, for this embankment there are no detailed field measurements of settlements and excess pore water pressures in the ground. Only the overall geometry before and after failure are known (Fig. 3). Therefore, the numerical results are mainly compared with each other in order to investigate the effects of the strain-softening. This is achieved by considering: (1) deformation and shear strain contours; (2) stress paths for some typical points within the soil and the shear stress level (SSL), defined as the ratio of the mobilized shear stress divided by the corresponding shear strength; and (3) the excess pore water pressures generated in the ground. Comparisons between the overall predicted displacements and the measured displacements have also been made.

6. Predictions

6.1. Deformations

The values of deformation presented here exclude those deformations induced by excavation of the old canal. The settlement versus time curves at points A–H (Fig. 11) are given in Fig. 12a–h. In Fig. 12a, the results of using lower values of hydraulic conductivity (k) (half of the values in Table 3) and higher k values (1.5 times of the values in Table 3) are also included for comparison. The deformed meshes at the end of the analysis are compared in Fig. 13a and b. The field survey results after the failure have been incorporated into Fig. 13 as a reference. It can be seen that the magnitudes as well as the pattern of settlements are significantly different for the softening and the no-softening cases. The obvious difference appears at about 30 days of elapsed time (after placing 1.0 m of fill material). After the embankment construction, small consolidation settlement increments were induced at all points except E and F in the no-softening case. However, for the softening case, it was predicted that after the embankment construction progressive failure induced much larger settlements under the embankment at points A, B and C. Even during subsequent consolidation some elements softened and transferred their load to surrounding elements, and gradually increased the size of the failure area and the magnitude of the shear deformations. Although settlements were not monitored in detail in the field, the ground surveying conducted before and after the failure (Fig. 3a) indicate that the embankment settled about 0.5 m. Even the FEM analysis that considered strain-softening had limitations in simulating the post-failure deformation, but nevertheless, the results of the softening case (Fig. 12a) are closer to the estimated field settlements. Fig. 12a also indicates that before the end of the embankment construction, the higher the k values, the larger the consolidation settlement, but both the lower and higher k value cases result in slightly larger final settlements. A higher k value will increase the rate of consolidation and result in stiffer and stronger ground before softening commences. Therefore, the lower k value case tends to result in larger softening-induced deformation. However, since the amount of strength reduction during the softening process is specified as a percentage of the strength at the beginning of the softening, a higher strength before the start of softening means a larger amount of strength reduction during the softening process, and it can also increase the softening-induced deformation. For point D, at close to the end of the embankment construction, the deflections started to rebound slightly. As shown in Fig. 13b for the softening case, on the embankment side, soil elements above about 4.5 m depth from the ground surface moved downward as well as to the right (toward the canal). This kind of deformation pattern appears to correspond to some unloading at point D resulting in some rebound. On the excavation side, at points E and F, progressive failure caused large amounts of heaving in the softening case. The amount of heave is comparable with the magnitude of settlement at points A and B. Again, from the survey results before and after the failure, about 1.0 m of heaving at the bottom of the canal can be estimated, and the results of the softening case are closer to this estimate. In contrast, at point H after the embankment construction, the deformation direction changed from heaving to settling. This is considered to be due to consolidation or perhaps the rightward movement of the embankment body may have increased the load acting in the vertical direction at this point.

A comparison of the simulated lateral displacements at the location of the wooden-pile wall (toe of the embankment) at the end of analysis is given in Fig. 14. At about 2 m depth, the softening case produced about twice the lateral displacement of the no-softening case, and the predicted value is closer to the field movement of the piles estimated by the location and the inclination of their heads. From the results of the softening case, a clear indication of the formation of a potential slip surface at about 4.0–4.5 m depth can be observed. Below this depth, the lateral displacements in the no-softening case are generally larger than in the softening case because the potential slip surface promotes the separation of the sliding body and the soil mass below it. For the softening case, the results of the limited parametric study on the effect of

hydraulic conductivity (k) indicate that the lower the k values, the larger the lateral displacements because of the lower shear strength in the ground. Although it seems that the under-prediction of the lateral displacement may be due to possible over-estimation of the k values, we believe the k values adopted are reasonable and the main reason for the under-prediction is more likely to be the inability of the proposed method to simulate post-failure deformation.

The shear strain contours at the end of the analysis are compared in Fig. 15a–c. Fig. 15c shows the result of using the coarser mesh for the softening case. Comparing Fig. 15b and c indicates that the solution for this strain-softening problem, like most cases of strain-softening, is mesh size dependent, and a finer mesh is desirable. From Fig. 15a and b, it can be seen that for the no-softening case, the simulated maximum shear strain under the embankment is about 8% and there is a small zone under the canal

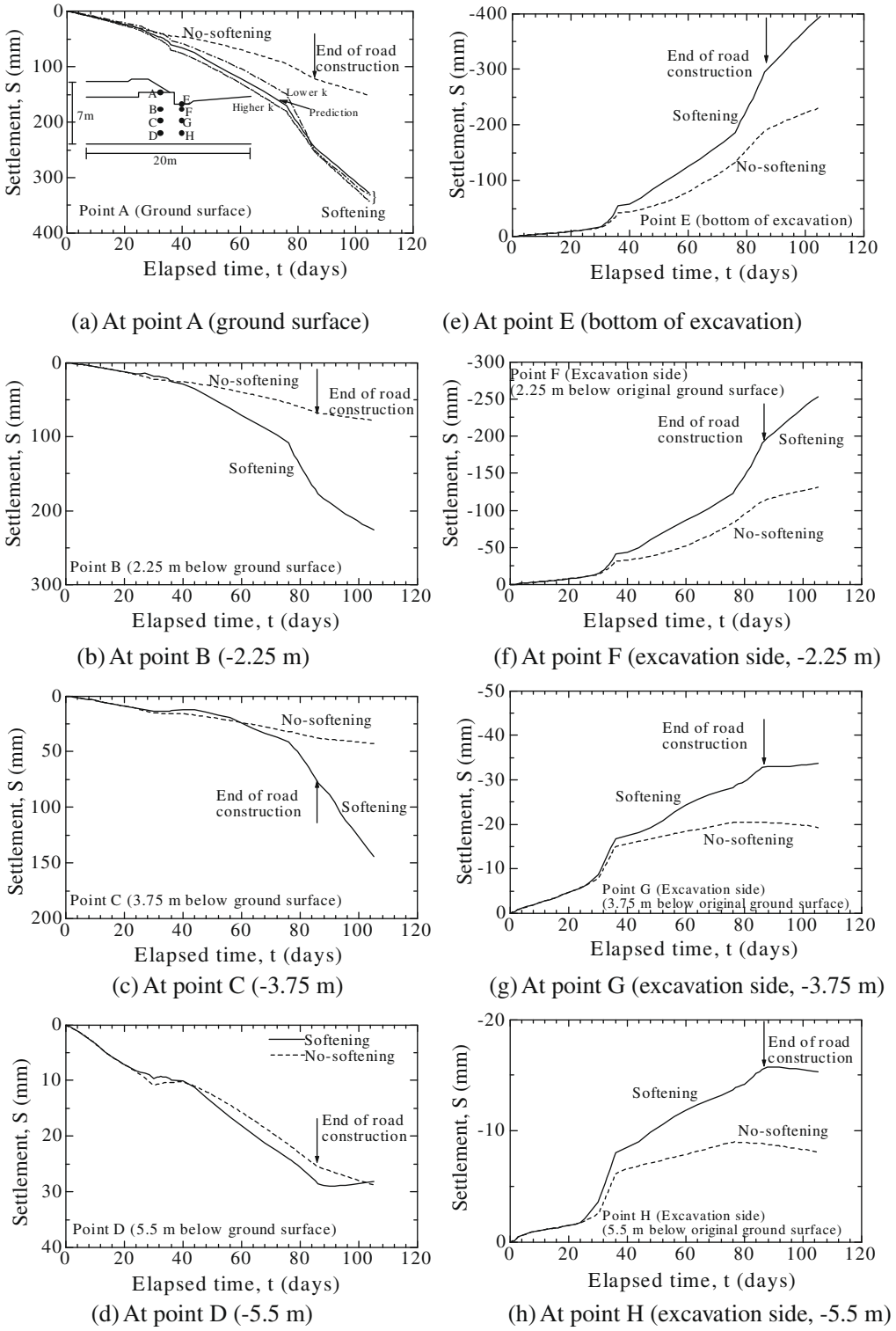

Fig. 12. Comparison of settlements at points A–H.

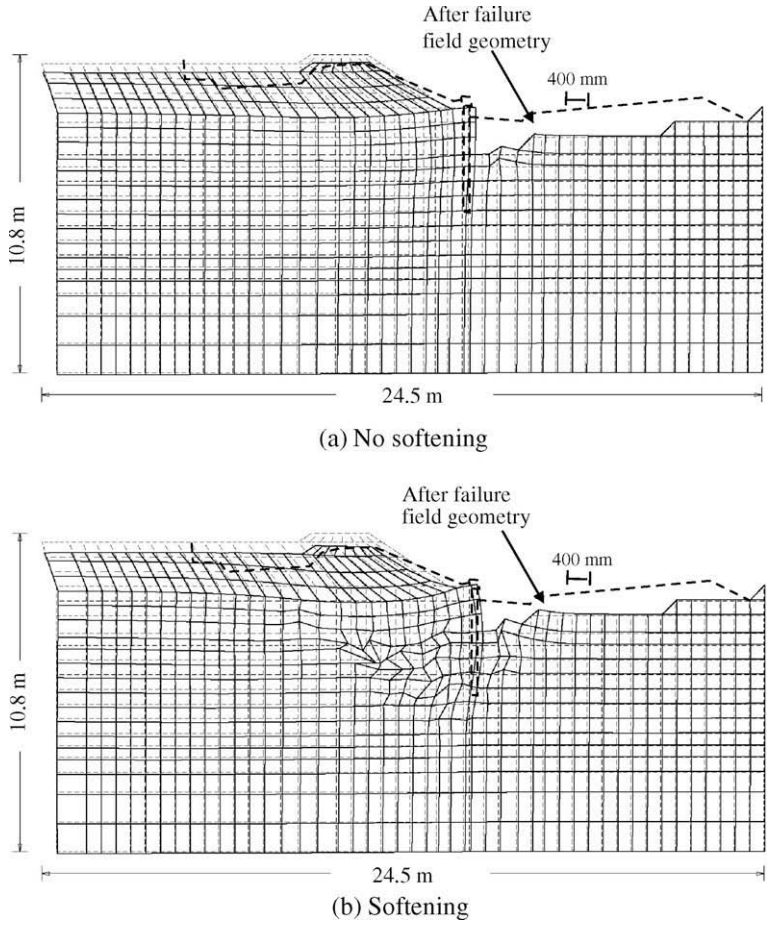

Fig. 13. Comparison of deformed meshes at the end of analysis.

where the shear strains are larger than 9%. However, for the softening case there are larger zones where the shear strains are more than 9% both under the embankment and the canal, and they are connected to form a potential slip surface. Fig. 15a and b indicate that during softening, the softened elements not only transfer load to the surrounding elements, but also result in shear strain localization. For the softening case (Fig. 15b), there are zones of larger shear strain (>9%), but in the foundation the 1% shear strain zone is smaller than that of the no-softening case (Fig. 15a). In the fill, the 1% shear strain zone is larger for the softening case than for the no-softening case, indicating the development of a potential failure surface through the fill material. Furthermore, in Fig. 15, the 1–2% shear strain zone for the non-softening case is larger than that of the softening case, which also indicates strain localization occurring in the softening case. Fig. 15 presents the results at the end of the analysis, showing that the large shear strain zone has already propagated into a large area above the predicted potential failure surface. In earlier stages, when the potential failure surface develops as a result of progressive failure, the shear zone is more localized into a narrow band.

The results presented above indicate that the simulated potential failure surface is at about 4.5 m depth, which agrees with slip circle analysis result obtained using Bishop's method, but shallower than the estimated field failure surface suggested by Takayama et al. [14].

6.2. Stress paths and contours

To check the strain-softening process, the effective stress paths at points B, C, and D are compared in Fig. 16a and b, and they in-

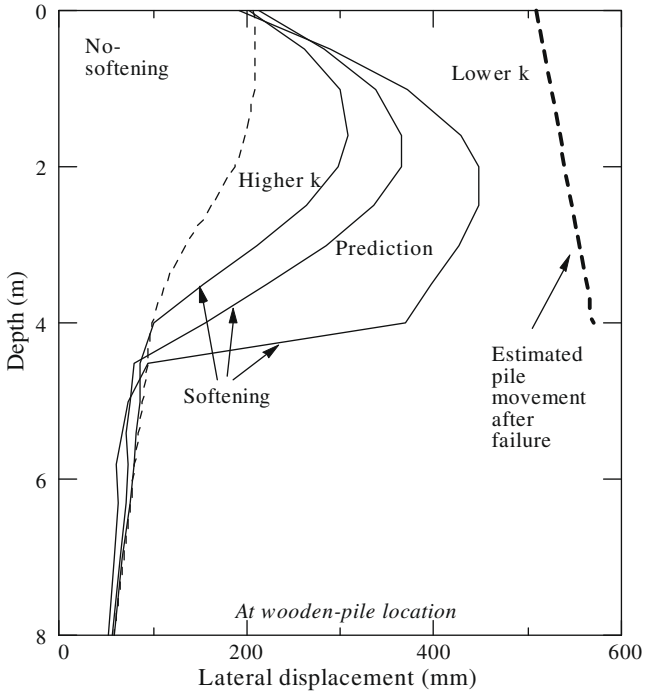

Fig. 14. Comparison of lateral displacement at wooden-pile location at the end of analysis.

clude the stress changes that occurred during excavation of the old canal. For the no-softening case (Fig. 16a), the stress path at point B reached the CSL and stayed there. For points C and D, during the embankment construction process, the stress path moved toward the CSL, but after that it moved almost horizontally (increasing the mean effective stress and maintaining the deviator stress). However, for the softening case (Fig. 16b), at points B and C, the stress path softened along the CSL. At point C, there is a period during which the stress path moved away from the CSL and then progressive failure transferred some shear load to it and the stress path moved back to the CSL and then it softened along the CSL. The progressive failure process also caused the stress path at point D to move toward the CSL not quite reaching it.

The stress paths at points F, G and H are compared in Fig. 17a and b. For both the softening and the no-softening cases, the effective stresses followed close to the k_0 line during excavation of the old canal. During the subsequent embankment construction there are some differences at points F and H. At point F, after the first layer of fill construction (1.0 m thick) and especially during the subsequent deepening of the canal, the induced extension load brought the stress path above the CSL where it probably reached the yield surface. As a result of adding the final layer of fill material (0.5 m thick) and construction of the road embankment, the stress path moved close to the CSL, and further heaving possibly caused tensile straining reducing both p' and q, bringing the stress state toward the origin (zero stress state). For the softening case, during the consolidation process after the embankment construction, the stress state reached the CSL and after the enforced softening the strength reduced to 70% of the value of q_{cs} when the CSL and yield surface were first simultaneously encountered. As required, the stress state then remained at this strength level. For the no-softening case, obviously there was no enforcement of softening and the stress state moved closer to the origin. At point H, for the no-softening case the stress state moved toward the CSL almost vertically

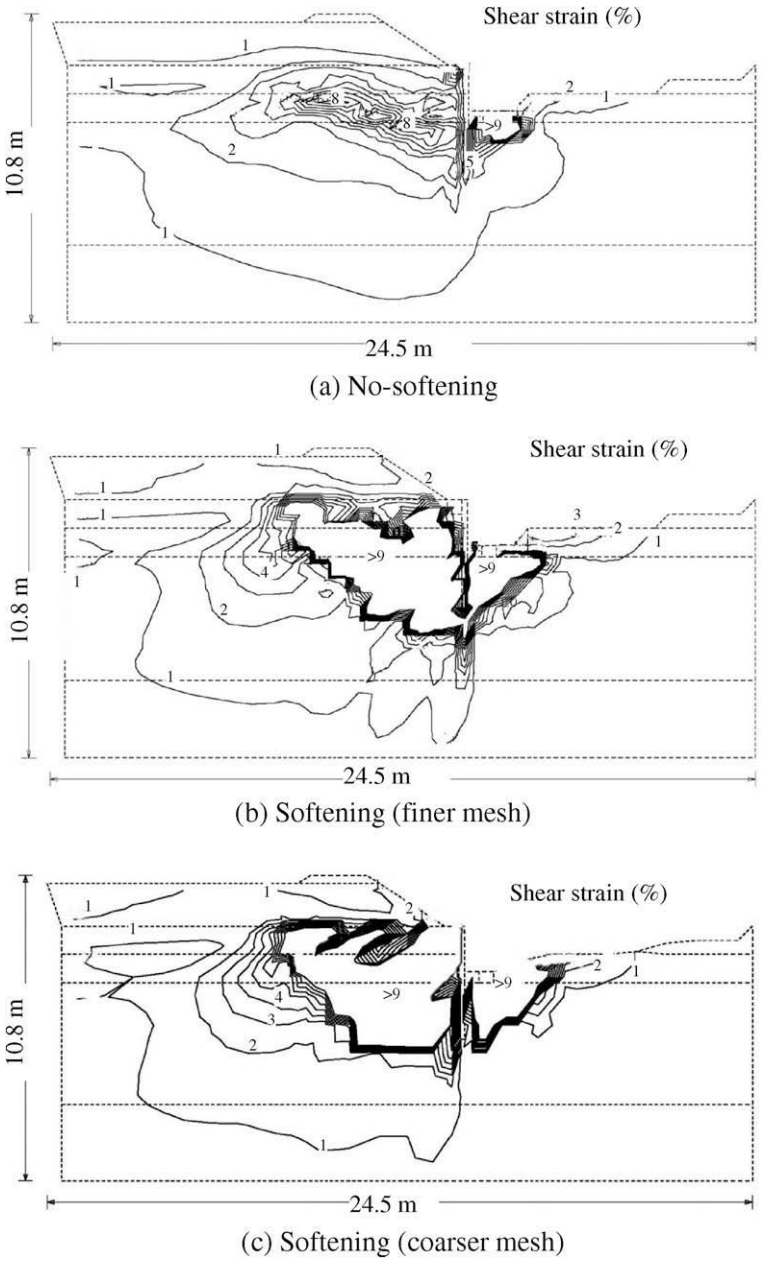

Fig. 15. Comparison of shear strain contours at the end of analysis.

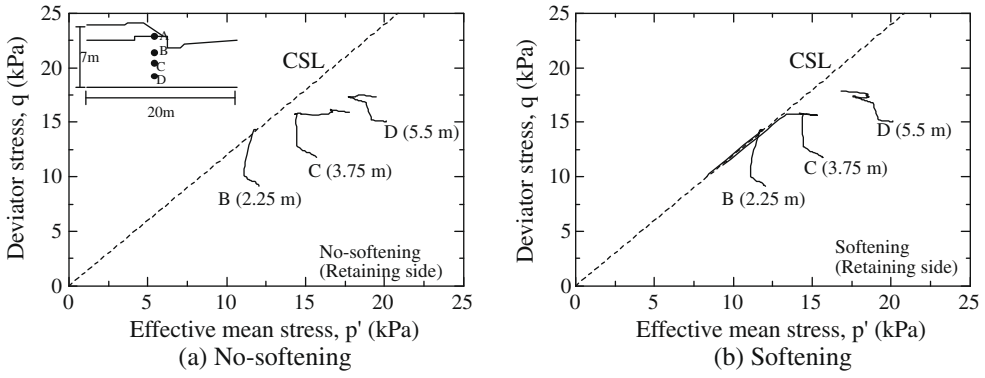

Fig. 16. Stress paths at points B, C and D.

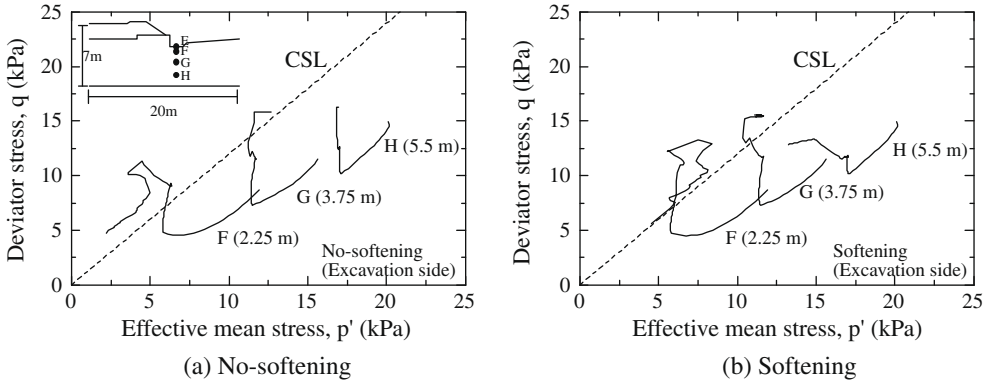

Fig. 17. Stress paths at points F, G and H.

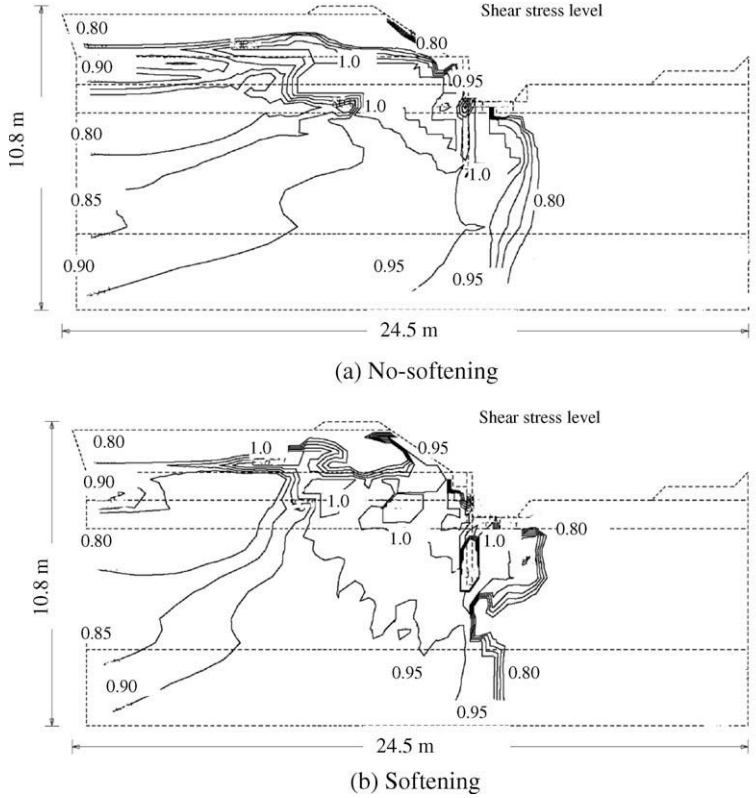

Fig. 18. Comparison of shear stress levels at the end of analysis.

(extension loading), but for the softening case, it moved leftward due to the progressive softening process.

The shear stress levels (SSLs) are compared in Fig. 18a and b for the no-softening and the softening cases at the end of the analysis, respectively. The inverse of SSL is the local factor of safety (FS) with respect to shear failure. There are two noticeable differences, one is that the zones where SSL = 1.0 and 0.95 under the embankment are larger for the softening case than they are in the no-softening case, and the other is that for the softening case there is a small zone where SSL = 1.0 in the embankment fill. This suggests that softening has caused an increase in the overall size of the failed zone.

6.3. Excess pore water pressures

Normally, softening processes increase the excess pore water pressures (u) in the ground. The simulated variations of u for points A–D, and F–H are compared in Fig. 19a–g. For point E, after the canal excavation, a drainage boundary was adopted and so this point is

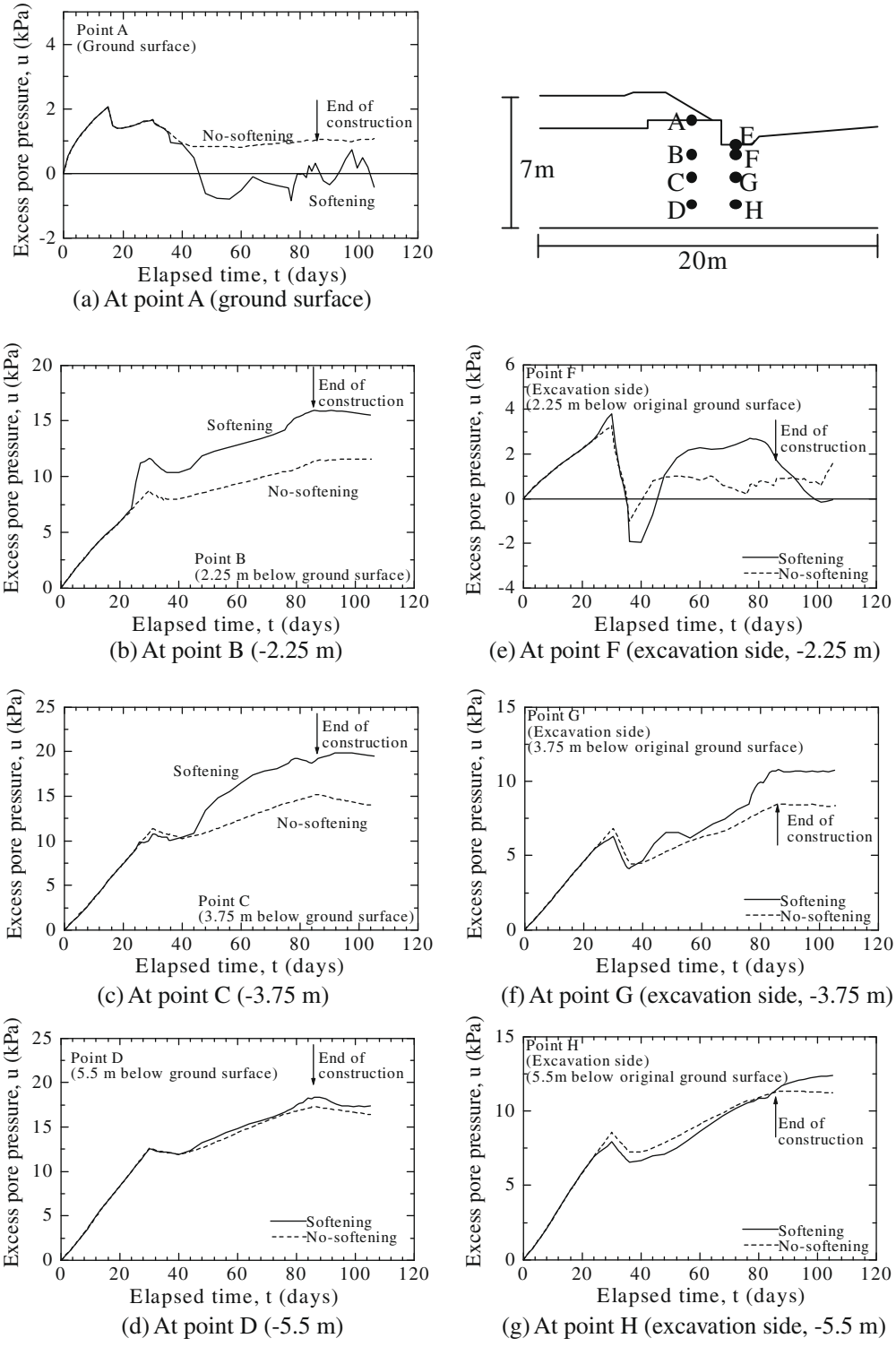

Fig. 19. Comparison of excess pore water pressures.

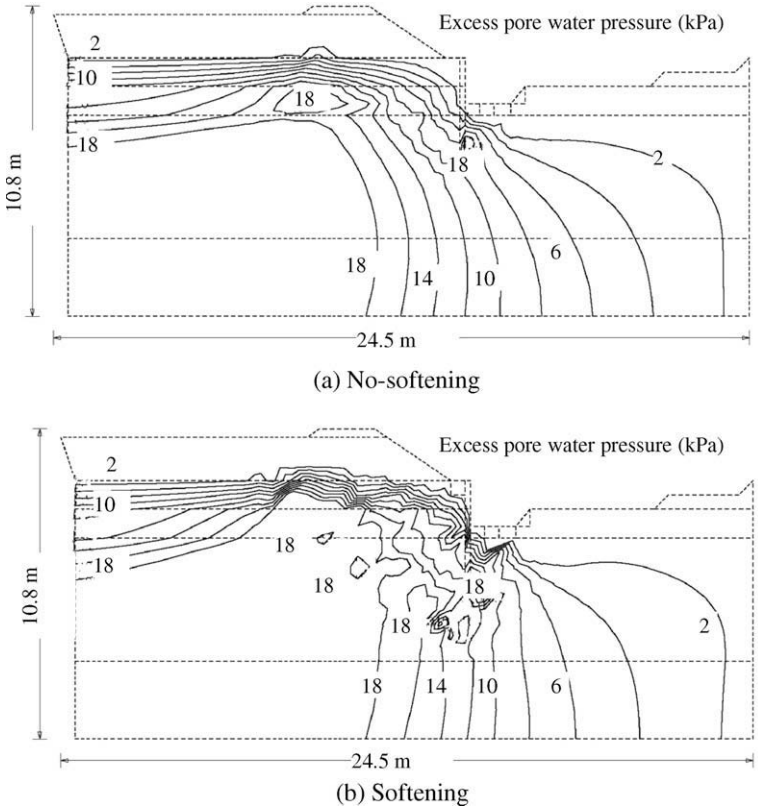

Fig. 20. Comparison of the contours of excess pore water pressure at the end of the embankment construction.

excluded. It can be seen beneath the embankment that except for point A the values of u for the softening case are indeed higher than those of the no-softening case. After an elapsed time of about 40 days, at point A the softening case simulated a value of u close to zero and lower than the no-softening case. This is probably due to the larger lateral displacements inducing tensile straining at point A, thus reducing the value of u. At points B and D after the embankment construction, there is no increase of u. This is because at point B the specified softening was completed before the end of the embankment construction and at point D, the stress states had not reached the CSL and so no-softening occurred (Fig. 16a). At point C after the embankment construction, there was a small increase of u, which indicates that some softening occurred at point C after the embankment construction. On the excavation side at points G and H, the final u values are higher for the softening case than for the no-softening case. At point H, after embankment construction, there is some increase of u indicating that progressive failure has caused the transfer of some shear load consistent with the stress path movement towards the CSL, as shown in Fig. 17b.

The excess pore water pressure contours at the end of embankment construction are compared in Fig. 20a and b for the no-softening and the softening cases, respectively. It can be seen that for the softening case the zone with u values equal to or larger than 18 kPa is larger than that for the no-softening case. The results presented in Figs. 19 and 20 clearly demonstrate that the process of strain-softening and induced progressive failure has involved a gradual increase in the excess pore water pressures in the softening zone.

7. Conclusions

A pragmatic strain-softening model proposed by Chai et al. [7], based on the Modified Cam Clay model, was applied to the simulation of progressive failure of an embankment on a sensitive clay deposit at Saga in Japan. By comparing the results of analyses with and without enforced strain-softening, the following conclusions can be drawn.

(1) The strain-softening method is capable of simulating the progressive failure mechanism for the embankment on the soft clayey deposit. For the case considered, progressive failure developed after the embankment construction and induced large shear deformations which finally led to failure of the embankment. Therefore, for such deposits progressive failure induced by strain-softening should be considered in design, and the residual strength of the deposit may have a significant influence on the overall factor of safety of the construction.
(2) Detailed analyses of the excess pore water pressures, shear strains and shear stress levels induced in the foundation soil indicate that the strain-softening process involved the buildup of excess pore water pressure, promoted strain localization and was associated with the development of a larger failure zone.

Acknowledgements

Dr. R. Nakamura of Shinwa Techno Co. Ltd., Japan, provided the results of the failed embankment analyzed in this study, and information about the structure of the wooden-pile and concrete-beam system constructed at the toe of the embankment. His generous assistance is gratefully acknowledged. The authors also wish to thank the anonymous reviewers of this paper for their very helpful comments.

References

[1] Adachi T, Oka F, Hirata T, Hashimoto T, Nagaya J, Mimura M, et al. Stress–strain behavior and yielding characteristics of Eastern Osaka clay. Soils Found 1995;35(3):1–13.

[2] Britto AM, Gunn MJ. Critical state soil mechanics via finite elements. Ellis Horwood Limited; 1987. p. 486.
[3] Carter JP, Liu, MD. Review of the structured Cam clay model, soil constitutive models: evaluation, selection and calibration. ASCE, Geotechnical Special Publication No. 128; 2005. p. 99–132.
[4] Chai J-C. Interaction between grid reinforcement and cohesive-frictional soil and performance of reinforced wall/embankment on soft ground. PhD Dissertation. Asian Institute of Technology, Bangkok, Thailand; 1992.
[5] Chai J-C, Miura N. Investigation on some factors affecting vertical drain behavior. J Geotech Geoenviron Eng, ASCE 1999;125(3):216–26.
[6] Chai J-C, Carter JP, Hayashi S. Vacuum consolidation and its combination with embankment loading. Can Geotech J 2006;43(10):985–96.
[7] Chai J-C, Carter JP, Hayashi S. Modeling strain-softening of clayey soils. Lowland Technol Int, Int Assoc Lowland Technol 2007;9(2):29–37.
[8] Davis EH, Booker JR. The effect of increasing strength with depth on the bearing capacity of clays. Géotechnique 1973;23(4):551–63.
[9] Japanese Society of Civil Engineering (JSCE). Civil engineering handbook. Gi-Hou-Dou Press; 1964 [in Japanese].
[10] Park YM. A research on the mechanical properties of lowland marine clay and vertical drain improvement method. Doctor of Engineering Thesis. Saga University, Japan; 1994.
[11] Potts DM, Dounias GT, Vaughan PR. Finite element analysis of progressive failure of Carsington embankment. Géotechnique 1990;40(1):79–101.
[12] Roscoe KH, Burland JB. On the generalized stress–strain behavior of 'wet' clay. In: Heyman J, Leckie FA, editors. Engineering plasticity. Cambridge University Press; 1968. p. 535–609.
[13] Sloan SW. Substepping schemes for numerical integration of elasto-plastic stress–strain relations. Int J Numer Meth Eng 1987;24:893–911.
[14] Takayama M, Nakamura R, Muraoka Y. Failure of embankment-canal slopes on soft subsoil and the strength recovering of the soft foundation soil – a case at Kouhoku area. Technical Report of the National Research Institute of Agricultural Engineering, Ministry of Agriculture and Forestry, Japan, Series E, No. 9; 1973. p. 1–12.
[15] Tanaka H, Shwakoti DR, Mishima O, Watabe Y, Tanaka M. Comparison of mechanical behavior of two overconsolidated clays: Yamashita and Louiseville clays. Soils Found 2001;41(4):73–87.
[16] Taylor DW. Fundamentals of soil mechanics. New York: John Wiley & Sons Inc.; 1948.